

# Evolution of interfacial dislocation network during low-stress high temperature creep of particle strengthened alloy system using discrete dislocation dynamics

Tushar Jogi<sup>a</sup>, Saswata Bhattacharya<sup>a,\*</sup>

<sup>a</sup>*Department of Materials Science and Metallurgical Engineering, Indian Institute of Technology Hyderabad, Kandi, Sangareddy-502285*

---

## Abstract

We use three-dimensional discrete dislocation dynamics (DDD) simulations to study the evolution of interfacial dislocation network (IDN) in particle-strengthened alloy systems subjected to a constant stress at high temperatures. We have modified the dislocation mobility laws to incorporate the recovery of dislocation network by climb. The microstructure consists of uniformly distributed cuboidal inclusions embedded in the simulation box. Based on the systematic simulations of IDN formation as a function of applied stress for prescribed inter-particle spacing and glide-to-climb mobility ratio, we derive a relation between effective stress and normalized dislocation density. We use link-length analysis to show self similarity of immobile dislocation links irrespective of the level of applied stress. Moreover, we modify Taylor's relation to show the dependence of effective stress on ratio between mobile to immobile dislocation density. We justify the relation with the help of a theoretical model which takes into account the balance of multiplication and annihilation rates of dislocation density.

*Keywords:* discrete dislocation dynamics, creep, superalloy

---

The dislocation movement and their interactions with underlying microstruc-

---

\*Corresponding author

*Email addresses:* ms14resch11003@iith.ac.in (Tushar Jogi), saswata@iith.ac.in (Saswata Bhattacharya )

ture decide the life of  $\gamma'$  strengthened Ni-base superalloys. These alloys exhibit exceptional mechanical strength at high temperature because of precipitation strengthening where coherent  $\gamma'$  precipitates impedes the motion of dislocation through matrix [1]. Many TEM observations have revealed the formation of dense interfacial dislocation network (IDN) around cuboidal  $\gamma'$  precipitates during low to intermediate stresses ( $100 - 550 MPa$ ) and high homologous temperature ( $850 - 1050^\circ C$ ) creep deformation of these materials [2, 3, 4, 5, 6, 7]. Several groups have reported that the evolution of the dense network of dislocation govern the recovery process during creep. Over the years, researchers have developed sophisticated electron microscopy techniques to investigate the formation of dislocation networks high temperature creep [8, 9, 10, 11, 12, 13]. Most of these investigations show the IDN over the surface of precipitates. They have proposed that such network formed as a result of dislocation reactions. A steady state high temperature creep evolution in particle strengthened alloy system can be visualized as development of three dimensional IDN network and consecutive occurrence of strain hardening and recovery events [14, 15, 16]. Attractive junctions formed due to dislocation reactions contribute to strain hardening. Under the influence of applied stress, eventually the some of the attractive junctions break down and released dislocation gives rise to recovery event. Further, the released dislocation again conjoins the network and consecutive strain hardening and recovery events are repeated.

Most studies conclude that the characteristics of the dislocation network is a complex byproduct of applied stress, lattice misfit, and interparticle spacing [8, 17]. Zhang et.al. [11] have studied the role of sign and magnitude of lattice mismatch between  $\gamma$  and coherent  $\gamma'$  precipitates on the mobile characteristics of the network. Larger negative misfit transforms more mobile hexagonal morphology to less mobile square network. In some cases, dislocation network contains a mixture of square and hexagonal morphology [7, 18]. Several studies based on computer simulations in three dimensions have been conducted to understand the mechanisms of formation of IDN and its role during the high temperature creep at continuum as well as atomic length scales. Yashiro et. al. [19] investi-

gated the stability of interfacial dislocation network and introduced a softening mechanisms of dislocation penetration through precipitate by using back-force model in DDD framework. Further, using back-force model, Huang et. al. [20] investigated the effect of precipitate size, channel width, and shape of precipitate (spherical and cuboidal) on formation of dislocation network and hardening rate. In another work, Haghghat et. al. [21] reported a DDD model wherein the dislocation-precipitate interaction forces and the conservative climb of edge dislocation as recovery mechanism during high temperature creep is taken into account. Furthermore, Liu et. al. [22] extended the model by incorporating misfit stresses to understand formation of different dislocation junctions (e.g. Lomer junction, Hirth junction, glissile junction, etc.) arising due to dislocation reactions and studied its effect on dynamic recovery during high temperature creep. Using DDD simulations, Gao et. al. [23] have investigated the effect of sign of lattice misfit and sign of applied stress (compressive or tensile) on deformation mechanisms and anisotropy of deformation in  $\gamma$  channels.

Zhu et. al. [24] studied the formation of interfacial dislocation network using molecular dynamics simulations where stability of dislocation network was shown to be due to the formation of Lomer-Cottrell junctions and dislocation network provides resistance to matrix dislocation to penetrate the particles.

Many studies have analysed the dislocation network using link-length distribution model where the statistical distribution of dislocation link length gives the useful measures of high temperature creep [25, 26, 27, 28]. There exists a stress dependent threshold dislocation link length in the distribution below which all the dislocation links are sessile whereas remaining region consists of mobile dislocation links. A steady state of dislocation network is realised when the dislocation link distribution is time independent. Thus, the ratio of mobile dislocation density to sessile dislocation density is constant at steady state. Sills et. al. [29] reported that dislocation link length follows an exponential distribution using DDD simulations of strain hardening in single crystals at room temperature and showed that the Taylor's relation is obeyed in DDD simulations. However, at high temperatures (above  $0.5T_m$ ) the validity of Taylors'

relation is not known with certainty [30].

In this work, we investigate the mechanisms for the formation of the interfacial dislocation network with the help of DDD method. Besides, we obtain the relationship between normalized dislocation density and normalized effective stress at the steady state high temperature creep and rationalize the relation theoretically.

The constant stress DDD simulations of microstructure comprising of uniformly arranged coherent ordered cuboidal inclusions are performed using modified ParaDis code. The ParaDis code is large scale massively parallel code to perform single crystal discrete dislocation dynamics simulation in FCC and BCC metals. The detailed algorithm and exhaustive exposition to method is available in references [31, 32]. The current open source ParaDis code takes into account dislocation-dislocation elastic interaction and dislocation elastic self-interaction. The detailed model description and governing equations are elucidated in reference [33]. However, we summarize the extensions in the following equations.

- ParaDis code has been extended to take into account particle-dislocation interaction forces arising due to order strengthening (refer eqn (1)).

$$f_{ij}^{particle} = \begin{cases} \frac{1}{2} \frac{\chi_{APB}}{\|\mathbf{b}\|} \|\mathbf{l}_{ij}\| \tanh\left(\frac{3(L-d_{min})}{L}\right) \mathbf{n}^s & d_{min} \leq L \\ 0 & d_{min} > L \end{cases} \quad (1)$$

Where,  $f_{ij}^{particle}$  is particle-dislocation forces on the segment connecting node  $i$  and  $j$ ;  $\chi_{APB}$  is APB energy;  $\mathbf{l}$  is dislocation segment vector;  $\mathbf{b}$  is Burger's vector;  $d_{min}$  is normal distance from dislocation node to surface of the particle;  $\mathbf{n}^s$  represents normal vector to the particle from node.

- For dislocation segments lying on  $\{111\}$  slip planes, octahedral slip and climb is considered. On the other hand, for dislocation segments not lying on  $\{111\}$  slip planes, only isotropic climb is considered (refer (2)). Climb mobility of mixed dislocation segment is described as interpolation between climb mobility of edge component of dislocation segment and glide

mobility of screw component of the dislocation segment (see eqn (3)).

$$B_{ij}(\xi) = \begin{cases} B^g m_i m_j + B^c n_i n_j + B^l t_i t_j, & \forall \mathbf{n} \in \{111\} \\ B^c \delta_{ij} + (B^g - B^l) t_i t_j, & \forall \mathbf{n} \notin \{111\} \end{cases} \quad (2)$$

where,  $B^g$ ,  $B^c$ , and  $B^l$  represents glide, climb, and line components of drag tensor  $B_{ij}(\xi)$  respectively;  $n_i$  represents slip plane;  $t_i$  represents dislocation line vector;  $\xi$  is tangential line vector to dislocation node;  $m_i = \epsilon_{ijk} n_j t_k$ , here  $\epsilon_{ijk}$  represents Levi-Civita symbol.

$$B^c = [(B^{ec})^2 \epsilon_{kij} b_i t_j \epsilon_{kpq} b_p t_q + (B^{sc})^2 (b_i t_i)^2]^2 \quad (3)$$

where,  $B^{ec}$  and  $B^{sc}$  are drag coefficients of edge and screw dislocation segments along slip normal direction. Here,  $B^{sc} = B^{sg}$  and  $B^{sg}$  represents the drag coefficient of screw dislocation along glide direction.

- The particle in the simulation box is constructed as superellipsoidal inclusions. Previous DDD studies [21, 22] have employ perfect cubes as inclusions, despite the fact that in reality the  $\gamma'$  particles are cuboidal shaped with rounded corners and edges. Superellipsoids are perfect geometric shapes belonging to superquadric family which are similar to cubes but with rounded corners and edges [34]. It can be described by following equation

$$T(x, y, z) = \left( \frac{x - x_0}{a} \right)^n + \left( \frac{y - y_0}{b} \right)^n + \left( \frac{z - z_0}{c} \right)^n \quad (4)$$

where,  $a, b$ , and  $c$  represents the half edge length of cuboid,  $n$  is the exponent which should be more than 3. Here we chose the value of  $n$  as 4.

The simulation box composed of eight equidistant cuboidal inclusion is considered to perform constant stress simulations. Parameters used for simulations are summarized in table 1.

Shear modulus, $\mu$	45 <i>GPa</i>
Poisson's ratio, $\nu$	0.37
Simulation box size	1 $\mu m^3$
Slip systems	[011](11 $\bar{1}$ ), [101]( $\bar{1}$ 11)
Burgers vector magnitude	0.25 <i>nm</i>
Particle sizes	400 <i>nm</i>
Channel Spacing	100 <i>nm</i>
Applied stress	300, 400, and 500 <i>MPa</i> along [001] direction
Glide to climb mobility ratio $M_g/M_c$	1/1000
Climb mobility $M_c$	0.01 $Pa^{-1}s^{-1}$

Table 1: Parameters used for different set of simulations

The applied stress levels of 300, 400, and 500 *MPa* are taken in order to understand effect of applied stress. Since the DDD simulations are computationally intensive, in order to obtain appreciable plastic strain, we have chosen higher levels of stresses compared to those used in standard creep experiments. In all set of simulations, we choose inter-particle spacing as 100*nm*. The initial dislocation lines are generated by the cross product of plane normal of particle surface and slip plane of the dislocation. The anti-phase boundary (APB) energy is chosen such that the dislocation segments are impervious to particles. We take the APB energy as 150 *mJ/m<sup>2</sup>*.

The initial dislocation configuration which is used for each set of simulation is shown in fig 1(a). Figure 1 (b) shows a three dimensional interfacial dislocation network formed around cuboidal particles. The intersection of non-coplanar dislocations produces triple junction (triple junction is the one where three dislocation segments meet) (see fig 1 (c)). The process is generally referred as zipping of junction. Under some critical stress, however, the unzipping of junction can take place wherein the triple junction can get destroyed. In some instances, since the triple junctions are more energetically favorable, even though quadruple junctions (quadruple junction is one where four dislocation

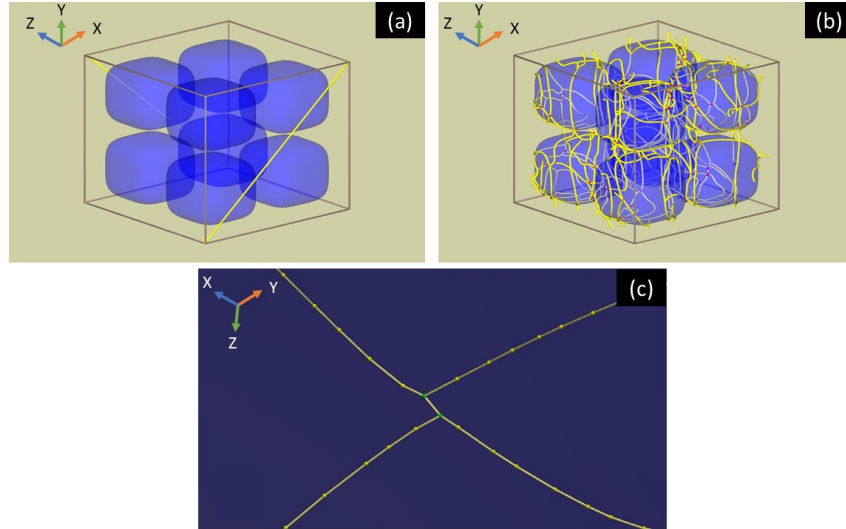


Figure 1: (a) Initial dislocation configuration. Two dislocation line of mixed character existing on  $[011](11\bar{1})$  and  $[101](\bar{1}11)$  slip systems. (b) The complex three interfacial dislocation network formed at stress level of  $300\text{ MPa}$ . The red color nodes represents triple junctions. (c) Formation of triple junctions by zipping at  $300\text{ MPa}$  when two dislocation segments intersects. The green color nodes represents the triple junction and segments held by two triple junction is newly formed sessile dislocation segment.

segments meet) are formed, it get converted into two triple junctions. It identifies the fact that triple junctions are most stable which constitutes the complex three dimensional IDN. Every two triple junctions formed hold the dislocation link possessing the Burgers vector which is given as per energetically favorable dislocation reaction shown below

$$\frac{1}{2}[0\bar{1}\bar{1}] + \frac{1}{2}[101] \rightarrow \frac{1}{2}[1\bar{1}0].$$

Thus, the Schmid factor associated with newly formed dislocation segment is zero. Consequently, the immobile links act as a bridge between four mobile dislocation segments. This leads to an implication that immobile dislocation links critically controls dynamics of interfacial dislocation network.

The IDN comprises mobile as well as immobile dislocations. The ratio of mobile to immobile dislocation length ( $\frac{\rho^m}{\rho^{im}}$ ) in the network is strongly influ-

enced by applied stress, as seen in fig 2(a). Figure 2(b),(c), and (d) show

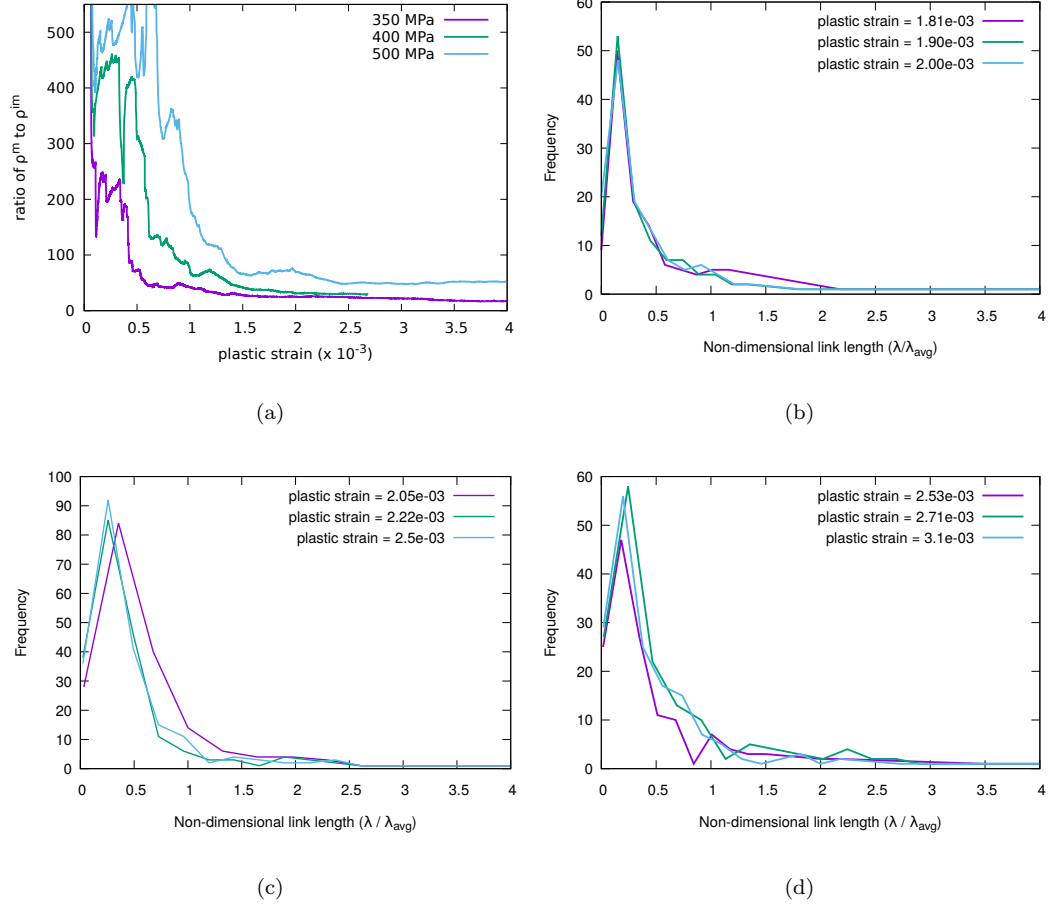


Figure 2: (a) Evolution of ratio of mobile dislocation density to immobile dislocation density ( $\frac{\rho^m}{\rho^{im}}$ ) against plastic strain. Steady state is reached when  $\frac{\rho^m}{\rho^{im}}$  tends to be constant. Increase in applied stress delays the onset of steady state. For 350 MPa, steady state is reached close to strain level of 0.00175, whereas for 500 MPa, steady state is reached at close to strain level of 0.0025. (b) Immobile link length distribution for the case of 350 MPa. (c) Immobile link length distribution for the case of 400 MPa. (d) Immobile link length distribution for the case of 500 MPa

the distribution of immobile link length. It is evident that the immobile link length distribution is fairly time independent after a critical strain is achieved. The immobile dislocation link length scales inversely with applied stress [35].

The mobile dislocations can easily multiply in simulations with higher applied stresses. Consequently, larger mobile dislocation density has more probability to collide with network to form junctions, and thus the large number of triple junctions of shorter length are formed at higher stresses.

Our simulation results show morphological features of interfacial dislocation network which bears good resemblance to that of the TEM observations. We have observed hexagonal loops over the surface of particles, comprised of dislocation segments with three different Burgers vector (refer fig 3 (a) ) [8, 9]. The formation of hexagonal loops can be explained as illustrated in fig 3 (b). In some instances, distorted hexagonal loops may form as an effect of immobile dislocation links being dragged due to motion of mobile dislocation links. Although, in case of 500 MPa, the loops consist of dislocation segments with three distinct Burgers vectors, the morphology appears to be more square like. This can be attributed to the shorter length of immobile dislocation lengths at applied stress of 500 MPa.

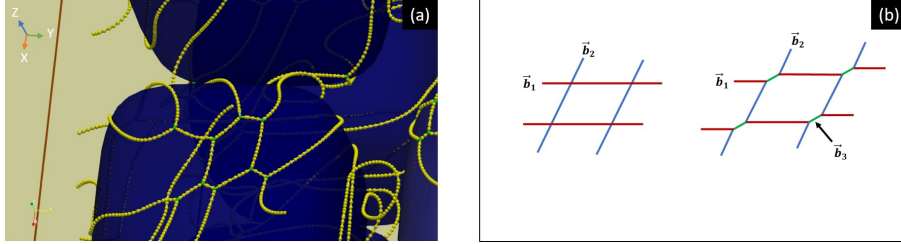


Figure 3: (a) Observation of hexagonal loops at stress level of 300 MPa. The loop is formed on face of precipitate oriented along [001] crystallographic direction. (b) Schematic representation of formation of hexagonal loops. When two parallel dislocation lines of Burgers vector  $\vec{b}_1$  and  $\vec{b}_2$  intersect, the trinode junction forms at intersection points. The junction formed has burgers vector  $\vec{b}_3$  which is different from other two segments. When the dislocation segments of  $\vec{b}_3$  is larger then the loop appears to be of hexagonal morphology whereas when it is shorter the morphology of loop appears to be close to square.

Additionally, we show the relationship between the normalized effective stress ( $\frac{\sigma_e}{\mu}$ ) and ratio of mobile to immobile dislocation density ( $\frac{\rho^m}{\rho^{im}}$ ). The effective stress is calculated by subtracting volume average back stress from

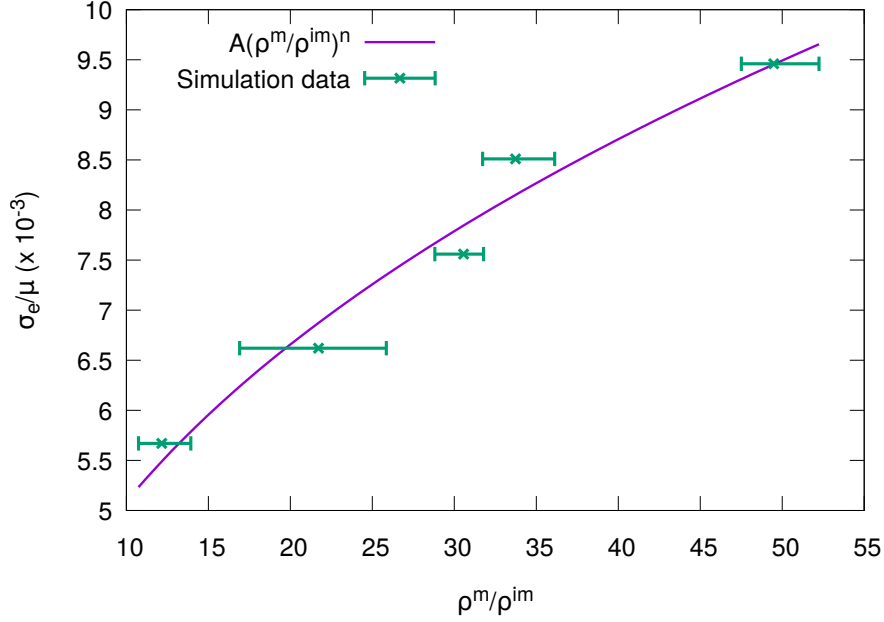


Figure 4: Effect of normalized applied stress on mobile to immobile dislocation density ratio. After fitting, the values of  $A = 2.087$  and  $n = 0.3872$  are obtained. The graph shows that ratio of mobile to immobile density scales non-linearly with applied stress.

applied stress. We invoke work hardening theory by Brown-Stobbs [36] to get an approximate measure of back-stress. The back-stress can be approximately given as product of shear modulus ( $\mu$ ), plastic strain( $\epsilon_p$ ), and volume fraction of particles. As per figure 2, after a critical strain is achieved, the  $\frac{\rho^m}{\rho^{im}}$  reaches a steady state values in all cases of different stress levels. Figure 4 represents the effect of normalized applied stress on ratio of mobile to immobile dislocation density. The average values of  $\frac{\rho^m}{\rho^{im}}$  after the steady state value is reached are obtained and fitted to equation 5.

$$\left(\frac{\sigma_e}{\mu}\right) = A \left(\frac{\rho^m}{\rho^{im}}\right)^n \quad (5)$$

After fitting, the values of  $A$  and  $n$  are obtained to be 2.087 and 0.3872 with standard error of 15.29% and 11.39% respectively. This result signifies

that the normalized effective stress scales non-linearly with ratio of mobile to immobile dislocation density. This result displays the deviation from Taylor's relation where the exponent to dislocation density is half. The deviation from the Taylor's relation can be attributed to high temperature recovery mechanisms present in the model. In the light of our results, the exponent to dislocation density can be rationalized as per ref [37] which explains the relationship between stress and dislocation density at high homologous temperature. Assume that the rate of increase in dislocation density is proportional to plastic strain rate, i.e.,

$$\frac{d\rho}{dt} = \alpha\dot{\epsilon} \quad (6)$$

where  $d\rho$  is change in dislocation density,  $\dot{\epsilon}$  is plastic strain,  $dt$  is time interval, and  $\alpha$  is proportionality constant. Further, the annihilation of dislocation density at high homologous temperatures is dependent on dislocation spacing. The dislocation spacing  $l_c$  can be approximated as  $l_c \approx \frac{1}{\sqrt{\rho}}$ . Hence, annihilation rate is given as

$$\frac{d\rho}{dt} = -\beta\frac{\rho}{l_c} = -\beta\rho^{3/2} \quad (7)$$

where  $\beta$  is proportionality constant. From equation (6) and (7), we obtain the net rate of change of dislocation density as

$$\frac{d\rho}{dt} = \alpha\dot{\epsilon} - \beta\rho^{3/2} \quad (8)$$

At steady state, where  $\frac{d\rho}{dt} = 0$ , from equation (8), we yield a relation between strain rate and dislocation density as

$$\dot{\epsilon} = \left(\frac{\beta}{\alpha}\right)\rho^{3/2} \quad (9)$$

The stress exponent of single crystal superalloy CMSX-4 varies from 3 to 7 at low to intermediate stresses and high homologous temperatures [38]. Hence

$$\dot{\epsilon} = K\sigma_e^{3-7} \quad (10)$$

where  $K$  is proportionality constant and  $\sigma_e$  is effective stress. Combining equations (9) and (10), we obtain the relation between effective stress and dislocation

tion density as

$$\sigma_e = \left( \frac{\beta}{\alpha K} \right)^{0.14-0.33} \rho^{0.21-0.5} \quad (11)$$

The exponent we obtained in equation (5) from simulation data lies in between the exponent shown in equation (11).

To summarize, three dimensional DDD simulations are performed by employing the modified ParaDis code. Our simulations show the formation of three dimensional IDN around cuboidal particles. The IDN is formed as a by-product of dislocation reaction. The characteristics of dislocation network morphology resembles well to the experiments. The attractive junction generated due to dislocation reactions provides the strength to the network. The immobile link length distribution is time independent after a critical strain is achieved at given applied stress. Moreover, we present the relationship between applied stress and ratio of mobile to immobile dislocation density and it agrees well with theoretical relation. The relation shows deviation from Taylor's relation.

## References

## References

- [1] R. C. Reed, The superalloys: fundamentals and applications, Cambridge university press, 2008.
- [2] A. Lasalmonie, J. L. Strudel, *Phil. Mag.* 32 (1975) 937–949.
- [3] M. Feller-Kniepmeier, T. Link, *Mat. Sci. and Engg. A* 113 (1989) 191–195.
- [4] T. Pollock, A. Argon, *Acta Metal. et Mat.* 40 (1992) 1–30.
- [5] S. Nategh, S. A. Sajjadi, *Mat. Sci. and Engg. A* 339 (2003) 103–108.
- [6] L. Carroll, Q. Feng, T. Pollock, *Metall. and Mat. Trans. A* 39 (2008) 1290–1307.
- [7] Y. Ru, S. Li, J. Zhou, Y. Pei, H. Wang, S. Gong, H. Xu, *Sci. rep.* 6 (2016) 29941.

- [8] T. Gabb, S. Draper, D. Hull, R. Mackay, M. Nathal, *Mat. Sci. and Engg.:* A 118 (1989) 59–69.
- [9] T. Sugui, Z. Huihua, Z. Jinghua, Y. Hongcai, X. Yongbo, H. Zhuangqi, *Mat. Sci. and Engg. A* 279 (2000) 160–165.
- [10] J. X. Zhang, T. Murakumo, Y. Koizumi, T. Kobayashi, H. Harada, S. Masaki, *Metall. and Mat. Tran. A: Phys. Metall. and Mat. Sci.* 33 (2002) 3741–3746.
- [11] J. X. Zhang, T. Murakumo, H. Harada, Y. Koizumi, *Scr. Mat.* 48 (2003) 287–293.
- [12] J. X. Zhang, J. C. Wang, H. Harada, Y. Koizumi, *Acta Mat.* 53 (2005) 4623–4633.
- [13] E. Alexander, L. Thomas, N. Gert, *J. of Micro.* 228 (2007) 110–117.
- [14] R. Lagneborg, *J. of Mat. Sci.* 3 (1968) 596–602.
- [15] R. Lagneborg, *Metal Sci. J.* 3 (1969) 18–23.
- [16] R. Lagneborg, *Metal Sci. J.* 3 (1969) 161–168.
- [17] Q. Yue, L. Liu, W. Yang, T. Huang, J. Zhang, H. Fu, *Mat. Sci. and Engg. A* (2018).
- [18] R. Field, T. Pollockf, W. Murphy, *Superalloys 1992* (1992).
- [19] K. Yashiro, M. Konishi, Y. Tomita, *Comp. Mat. Sci.* 43 (2008) 481–488.
- [20] M. Huang, L. Zhao, J. Tong, *Intl. J. of Plast.* 28 (2012) 141–158.
- [21] S. M. Hafez Haghghat, G. Eggeler, D. Raabe, *Acta Mat.* 61 (2013) 3709–3723.
- [22] B. Liu, D. Raabe, F. Roters, A. Arsenlis, *Acta Mat.* 79 (2014) 216–233.
- [23] S. Gao, M. Fivel, A. Ma, A. Hartmaier, *J. of the Mech. and Phy. of Solids* 76 (2015) 276–290.

- [24] Y. Zhu, Z. Li, M. Huang, *Comp. Mat. Sci.* 70 (2013) 178–186.
- [25] P. Lin, S. Lee, A. Ardell, *Acta Metall.* 37 (1989) 739–748.
- [26] L. Shi, D. Northwood, *J. of Mat. Sci.* 28 (1993) 5963–5974.
- [27] A. Ardell, M. Przystupa, *Mech. of Mat.* 3 (1984) 319–332.
- [28] P. Ostrom, R. Lagneborg, *J. of Engg. Mat. and Tech.* 98 (1976) 114–121.
- [29] R. B. Sills, N. Bertin, A. Aghaei, W. Cai, *Phys. Rev. Lett.* 121 (2018) 085501.
- [30] H. Mecking, U. Kocks, *Acta Metall.* 29 (1981) 1865–1875.
- [31] V. Bulatov, W. Cai, *Computer simulations of dislocations*, volume 3, Oxford University Press on Demand, 2006.
- [32] A. Arsenlis, W. Cai, M. Tang, M. Rhee, T. Opperstrup, G. Hommes, T. G. Pierce, V. V. Bulatov, *Model. and Sim. in Mat. Sci. and Engg.* 15 (2007) 553–595.
- [33] T. Jogi, S. Bhattacharya, *Trans. of the Indian Inst. of Metals* 69 (2016) 507–512.
- [34] A. Jaklic, A. Leonardis, F. Solina, *Segmentation and recovery of superquadrics*, volume 20, Springer Science & Business Media, 2013.
- [35] R. Madec, B. Devincre, L. P. Kubin, *MRS Online Proc. Lib. Arc.* 653 (2000).
- [36] L. M. Brown, W. M. Stobbs, *Phil. Mag* (1971) 1185–1199.
- [37] R. Horiuchi, M. Otsuka, *Trans. of the Japan Inst. of Metals* 13 (1972) 284–293.
- [38] Y. Kondo, N. Miura, T. Matsuo, in: *Mat. Sci. Forum*, volume 539, Trans Tech Publ, pp. 3100–3105.